

TURBULENCE IN THE SOLAR WIND MEASURED WITH COMET TAIL TEST PARTICLES

C. E. DEFOREST¹, W. H. MATTHAEUS², T. A. HOWARD¹, AND D. R. RICE³

¹Southwest Research Institute, 1050 Walnut Street Suite 300, Boulder, CO 80302, USA

²Department of Physics and Astronomy, University of Delaware, 217 Sharp Laboratory, Newark, DE 19711, USA

³Northwestern University, 633 Clark St., Evanston, IL 60208, USA

Received 2015 August 6; accepted 2015 September 8; published 2015 October 13

ABSTRACT

By analyzing the motions of test particles observed remotely in the tail of Comet Encke, we demonstrate that the solar wind undergoes turbulent processing enroute from the Sun to the Earth and that the kinetic energy entrained in the large-scale turbulence is sufficient to explain the well-known anomalous heating of the solar wind. Using the heliospheric imaging (HI-1) camera on board NASA's *STEREO-A* spacecraft, we have observed an ensemble of compact features in the comet tail as they became entrained in the solar wind near 0.4 AU. We find that the features are useful as test particles, via mean-motion analysis and a forward model of pickup dynamics. Using population analysis of the ensemble's relative motion, we find a regime of random-walk diffusion in the solar wind, followed, on larger scales, by a surprising regime of semiconfinement that we attribute to turbulent eddies in the solar wind. The entrained kinetic energy of the turbulent motions represents a sufficient energy reservoir to heat the solar wind to observed temperatures at 1 AU. We determine the Lagrangian-frame diffusion coefficient in the diffusive regime, derive upper limits for the small scale coherence length of solar wind turbulence, compare our results to existing Eulerian-frame measurements, and compare the turbulent velocity with the size of the observed eddies extrapolated to 1 AU. We conclude that the slow solar wind is fully mixed by turbulence on scales corresponding to a 1–2 hr crossing time at Earth; and that solar wind variability on timescales shorter than 1–2 hr is therefore dominated by turbulent processing rather than by direct solar effects.

Key words: comets: general – comets: individual (Encke) – solar wind – Sun: heliosphere – turbulence

Supporting material: animation

1. INTRODUCTION

The solar system is filled with two major types of supersonic outflowing solar wind that emanate from the solar corona and act collectively as a field-mediated fluid (Parker 1958; Neugebauer & Snyder 1966; Zirker 1977). The solar wind typically found near Earth, “slow wind” at 300–400 km s⁻¹, varies widely in both density and speed on scales from minutes to days, although the “fast” solar wind seen over the poles of the Sun does not (McComas et al. 2000). The origin of the slow solar wind is unknown, and understanding the nature of its variability provides critical clues. Models invoking steady flow along the edges of solar coronal holes, or plasma diffusion across the solar magnetic field (Raymond et al. 1997; Suess et al. 1998; Wang et al. 2007) do not produce a variable wind. Those invoking intermittent sources from magnetic “exchange reconnection” or myriad ejections of small plasmoids (Mullan 1991; Woo & Martin 1997; Fisk et al. 1999) suffer because transient structures seen with coronagraphs account for only a fraction of the mass of the solar wind (Wang et al. 1998). Determining why the slow solar wind is variable is a long-standing problem in heliospheric physics.

Understanding turbulence in the heliosphere is particularly important given its likely role in processing the solar wind (Cranmer 2012). Near Earth's orbit, solar wind variability has been well characterized by many spacecraft with in-situ instrumentation (Tu & Marsch 1995). Near the coronal base, where the solar wind originates, it has been possible to characterize at least some turbulent properties of the plasma using remote sensing techniques (Tu & Marsch 1995; Chae et al. 1998; Cranmer et al. 1999). Intermediate locations in the inner heliosphere are central to the development of turbulence

observed near 1 AU, but these locations have been only sparsely explored with single-point spacecraft measurements.

The solar wind density, magnetic field, and velocity at 1 AU have broadband spectral features reminiscent of turbulence (Kolmogorov 1941). Many other single-point features have also been well-described, yielding a plausible picture of an active, evolving medium (Matthaeus & Velli 2011) in which turbulence plays a role in modifying the solar wind and scattering cosmic rays (Jokipii 1966; Shalchi 2009). Turbulence therefore may make crucial contributions to establishing the global structure of the heliosphere (Breech et al. 2008; Elliott et al. 2012). But this work relies heavily on interpretation of single-point measurements from in-situ probes.

Single-point measurements provide little or no information about extended spatial structures, and no information at all about properties in the co-moving (Lagrangian) reference frame of the solar wind, as distinct from measurements made in a frame moving through the wind at hypersonic speed. By contrast, in theoretical research as well as laboratory hydrodynamic studies, it is well known that Lagrangian trajectories are necessary to determine how a turbulent fluid transports mass, structures, heat, momentum density, and other local material properties (Pope 2000).

Modern deep-field cameras and imaging techniques (DeForest et al. 2011) make it possible to image not only the dynamic solar wind itself but also comets and the local plasma clouds in comet tails. The latter can now be exploited as quantitative tracers of the wind flow, analogous to passive tracers in hydrodynamic laboratory experiments. Using image data from the *STEREO* mission's HI-1 instrument (Howard et al. 2008; Eyles et al. 2009), we have analyzed the ion tail of Comet

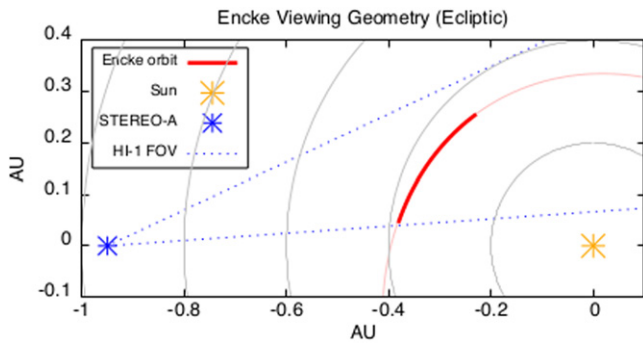


Figure 1. Head of Comet Encke passed through the *STEREO-A* HI-1 field of view, as seen from “above” the plane of the ecliptic in this diagram. The bold path shows viewing angles from 2007 April 21 to 28. As the comet moved away from the Sun in 3D, it moved closer to the Sun in 2D. Observed tail features were near 0.4 AU from the Sun throughout the observation.

Encke to measure turbulent motion in the co-moving frame of the solar wind itself.

The features in Encke’s ion tail arise from a combination of variation in the cometary mass loss rate (close to $3 \times 10^{28} \text{ s}^{-1}$; Mäkinen et al. 2001) and variation in the surrounding solar wind, which would break up even a smooth flow of mass from the comet. The tail particles are picked up by the solar wind via a complicated process of ionization, hydrodynamic interaction, and electromagnetic interaction (e.g., Gombosi et al. 1994). Several authors have attributed the clear variation of cometary ion tails to interaction with the solar wind (Alfvén 1957; Buffington et al. 2008; Clover et al. 2010; Jackson et al. 2013), including visual disconnections of the tail attributed to magnetic breaks associated with coronal mass ejections (Kuchar et al. 2004, 2008; Vourlidas et al. 2007). By tracking a complete ensemble of features from the comet, and quantitatively analyzing their motion across 10° of sky, we have exploited them as tracers of the surrounding solar wind.

In subsequent sections we describe our tracking technique, demonstrate that individual bright features in the ion tail act as “test particles” in the solar wind, and analyze their ensemble pairwise separation and relative speed as they propagated away from the comet. We exploit the pairwise separation analysis to visualize and quantify solar wind turbulence, resolving time/space ambiguities of existing in-situ measurements through direct tracking of particle trajectories. We conclude that the slow solar wind near Earth is fully mixed through turbulent eddies, and that variability observed by in-situ probes on timescales up to 1–2 hr is due primarily to this mixing rather than to variation in the solar source of the wind.

2. OBSERVATIONS AND REDUCTION

Comet Encke passed through the HI-1A field of view from 2007 April 21 through 2007 April 28 (Figure 1). In the study period the comet was outbound, between 0.35 and 0.39 AU. Encke is a short (3.3 year) period comet that typically presents with a remarkably well developed and well confined ion tail, and a fainter, straight dust tail. We tracked 230 individual features in the comet’s ion tail, across 10° of angle on the celestial sphere. A sample frame from this data set can be seen in Figure 2; and the entire image sequence with tracked datapoints is given in a supplementary digital movie, in the online version of this article. This broad angular range was enabled by deep background subtraction (DeForest et al. 2011) and the uniform 40 minute cadence of the *STEREO* data.

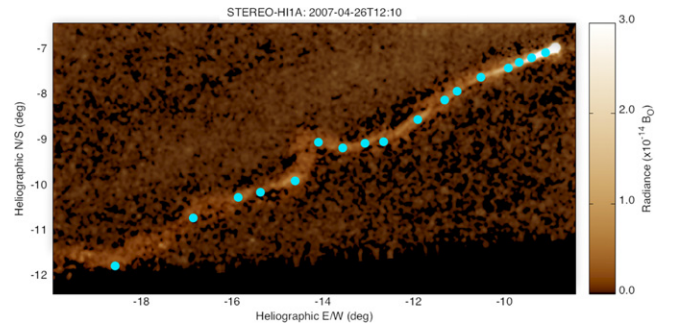


Figure 2. Sample frame from a photometric movie of Comet Encke passing through the HI-1 field of view shows the wide extent of the comet tail and several tracked features. We tracked a total of 230 features. See also the digital movie in the online version of this article.

(An animation of this figure is available.)

We downloaded the Level 2 (L2M and L2S) FITS-format photometric images that are available at the *STEREO* Science Center,⁴ for the date range 2007 April 21–28 inclusive. We developed a simple point-and-click graphical software tool to render adjacent frames on a screen and collect visual tracking data for each feature, across the two levels of processing. We used both the L2S (“Starfield-subtracted”) and L2M (“Motion-filtered”) data sets together, because the L2S processing preserves the comet head better, while the L2M processing has deeper dynamic range but omits slowly moving features such as the comet head. The tool produced feature locations as lists of pixel (x, y) coordinates in the image plane, versus time. We converted these locations to scientific (angular) coordinates using the included metadata in the *STEREO* images, and thence to projected image-plane linear distances using a fixed estimated distance of 0.6 AU from the observer to the object.

To verify that the visual feature tracking was correct, two of us (DeForest and Rice) independently tracked the tail and we compared the two derived datasets. The original set of 230 features identified by DeForest was corroborated by a second set of 170 features identified by Rice. We found that 153 of the features corresponded within 1 pixel in one or more frames, and of these all but two were good matches throughout the interval, with an rms error radius of 1.4 pixel (43 Mm in the image plane) across all frames where the same feature was found by both authors. In both of the exceptions, one author chose one of a pair of features near the start of the track and jumped to the adjacent feature in the fainter, distant portion of the comet tail—while the other did not. We accepted all 230 original features, and we calculate an expected value of 2–3 such mistracks in the final ensemble. The expected 3% effect in the ensemble statistics is included in our error analysis, but is negligible compared to other sources of error.

All subsequent analysis used the derived tracked location data, transformed to the fictional 2D “image plane” 0.6 AU from the observer, with the planar origin at the image location of the comet head.

3. ANALYSIS AND RESULTS

We carried out two forms of feature analysis. First, we executed a mean-across-features analysis to characterize the pickup dynamics of the features into the solar wind and establish under what conditions they act as test particles. Then

⁴ <http://stereo-scsc.nascom.nasa.gov>

we executed a pairwise ensemble analysis to characterize fluctuations in the particle dynamics and determine the local conditions in the solar wind flow.

3.1. Mean Transport and Pickup Dynamics

The comet tail plasma is not directly and instantly tied to the solar wind. The coupling is critical to both the physics of the tail plasma and the relationship between the solar wind and the observed dynamics of the tail. We measured this coupling empirically by fitting simple two-parameter models of the dynamics to the mean characteristics of the tracked data, to identify how well the best-fit models corresponded to the observed data. We considered two functional forms of pickup: *linear drag*, which is characteristic of electrodynamic pickup, hydrodynamics at low Reynolds number, or Epstein drag in tenuous media (Whipple 1972); and *quadratic drag*, which is characteristic of moderate-to-high Reynolds number hydrodynamics. Each model had two free parameters: a fixed radial solar wind speed and a time constant for pickup. As a null case, we also considered simple photon-pressure pickup in the absence of a solar wind. That is the dominant mechanism for accelerating the dust tail.

We began by calculating Encke’s trajectory in the data using its known orbital elements from the Minor Planet Center,⁵ and the pointing and spacecraft location metadata in the *STEREO-A* data. The a priori computed trajectory matched the observed image location of the comet head to within the resolution of the instrument. We launched a stream of simulated particles, at zero relative speed, from the comet’s orbital location at regular time intervals. We propagated the particles in a full 3D orbit with Keplerian dynamics modified by the particular functional form for each model, and projected them onto the image plane using the same transform as we used to place the comet head.

We constrained the models using the average characteristics of the ensemble of tracked features. We considered two dependent variables: the radial instrument-plane velocity v_r (in degrees per hour) and 2D angle from solar radial a (in degrees). We treated the tracked data as a time-independent ensemble and plotted the two dependent variables against the independent variable of image-plane distance from the comet, then smoothed using a running-mean filter. We used rms difference between the modeled v_r or a curve and the data derived curve, to drive a minimization algorithm and fit each model to the data.

We checked each model (linear versus quadratic drag) by producing two fits to each of the three models: one fit constrained only by v_r , and one constrained only by a . The level of agreement between the two fits is a qualitative measure of the model’s correctness, because v_r and a measure different aspects of the pickup physics. A model that captures the physics should yield similar fits when constrained either way, while one that does not should yield inconsistent fits across the two different measurable parameters.

The data and results of the fitting process are shown in Figure 3. Each row shows the results of one model. The top row shows that it is possible to adjust the model radiation pressure to match the exit angle of the tail or the radial

acceleration, but not both—this indicates (as expected) that the ion tail is not accelerated primarily by radiation pressure. The middle and lower rows show that the linear and quadratic models are each in moderate agreement and therefore are plausible descriptions of the pickup physics. The linear drag model is the best fit. The best-fit coupling time τ is 3–9 ks (1–3 hr). Constraining the linear model with both v_r and a together yields a τ of 6 ks.

We conclude that, on timescales longer than 6 ± 3 ks, the comet tail features act as test particles for the solar wind: on those timescales, the tail features follow the local short-term mean flow of the solar wind, while potentially experiencing random buffeting by parcels of solar wind plasma (“brownian motion”) on still shorter timescales.

3.2. Analysis of Tail Feature Separation

To characterize the dispersion of tail features into the solar wind, we considered the second-order positional structure function in 2D: $R^2(t) \equiv \langle \Delta x^2(t) + \Delta y^2(t) \rangle$, where t is the time since release by the comet, $(\Delta x(t), \Delta y(t))$ is the displacement vector in the image plane between a pair of features released at nearly the same time, and the average $\langle \dots \rangle$ is taken across the population of suitable feature pairs. We selected pairs of features that were within 6 pixels of one another at first detection of both features, and that lasted longer than 30 ks (~ 10 hr) before either feature was lost or exited the field of view. We linearly extrapolated the separation of each pair back to zero from its first two detection points, to identify a zero time reference roughly 2–3 ks before the first observation of each pair. We plotted this mean-square 2D distance R^2 versus time, as shown in Figure 4.

The first observation of a typical feature pair is at a spacing of 170–250 Mm (image-plane R^2 of 0.02–0.04 Gm²). R^2 grows linearly with elapsed time t for approximately the first 20 ks (5.5 hr) of evolution. We determined error intervals in Figure 4 from the standard error of the population mean at each location, added in quadrature to the detection threshold radius of 6 pixels (250 Mm).

This linear growth of mean-square separation is characteristic of a random walk or diffusive regime (Chandrasekhar 1943). It indicates that displacements by the wind of the features in each pair are uncorrelated, and we therefore find an upper bound of 250 Mm for the correlation length of any solar wind turbulence near the comet. This measurement is consistent with the range estimated from *Helios* in-situ data of 270–1200 Mm, 0.5–1 AU from the Sun: the correlation scale is expected to be proportional to distance from the Sun (Ruiz et al. 2014), and the comet tail is closer than the cited study range from *Helios*.

From the slope in the linear regime of Figure 4, we calculate the 2D diffusion coefficient as $D_{2D} = (1/2) (dR^2(t)/dt) = 5 \pm 0.1 \text{ Mm}^2 \text{ s}^{-1}$. That, in turn, corresponds to a 1D diffusion coefficient D_{xx} of $2.5 \pm 0.05 \text{ Mm}^2 \text{ s}^{-1}$.

The observed diffusive regime persists until the $R^2(t)$ relationship breaks to a subdiffusive $t^{1/4}$ relationship between approximately 15–25 ks (4–7 hr). At 5.6 hr, the center of the break, the rms 2D separation is 420 ± 12 Mm in the image plane. With the assumption of isotropic displacements, this corresponds to a 3D rms separation of 540 ± 15 Mm. The $t^{1/4}$ relationship holds until the features disappear from view. Although the population shrinks during the interval from 40–65 ks, the $t^{1/4}$ relationship holds among sub-populations

⁵ The International Astronomical Union’s Minor Planet Center publishes up-to-date ephemerides and orbital elements for thousands of solar system bodies. They can be found at <http://www.minorplanetcenter.net/iau/mpc.html>.

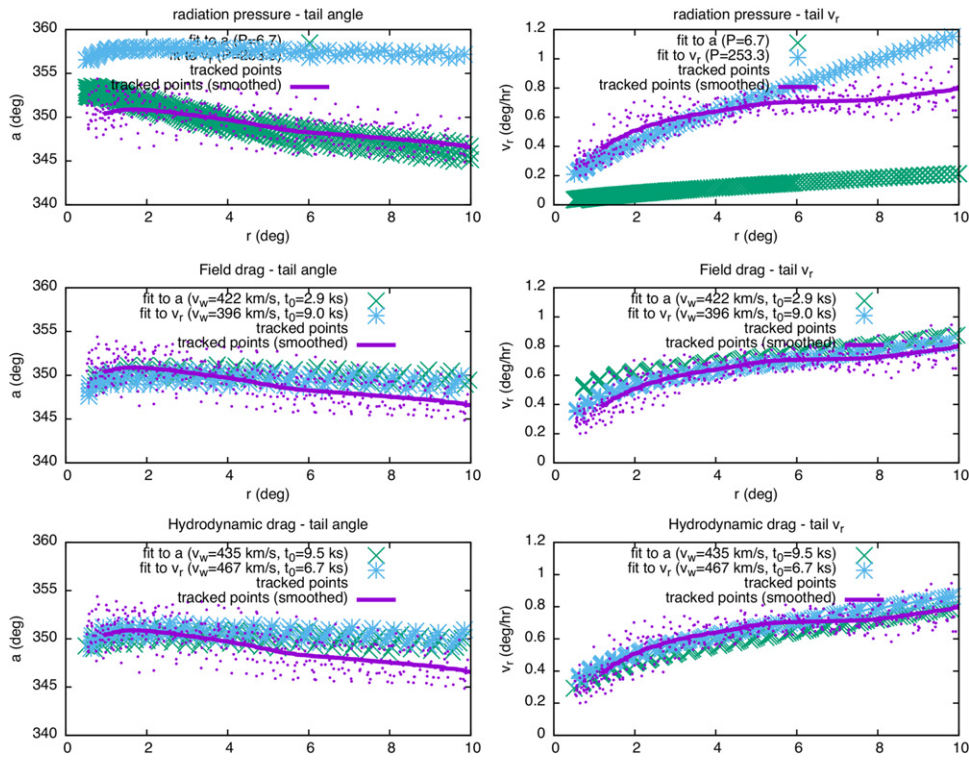


Figure 3. Multiple fits to the mean behavior of Encke’s tail determine the pickup mechanism. Purple: actual data points and median-smoothed fit target curve. Green: points fitted to the a curve. Blue: points fitted to the v_r curve. Top row: radiation pressure does not work and is inconsistent between a and v_r . Middle row: linear drag constrains radial speed and exit angle simultaneously. Bottom row: quadratic drag is plausible but inferior to the linear drag model.

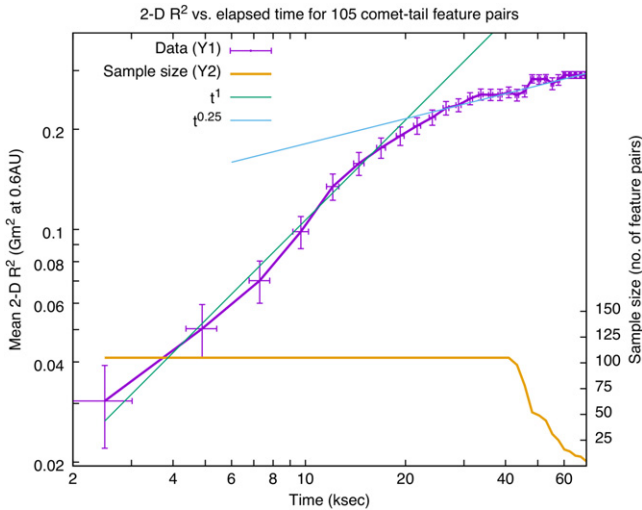


Figure 4. Evolution of the mean-square two-particle distance function R^2 vs. elapsed time, for comet-tail feature pairs that began within 250 Mm (6 pixels) of one another, reveals multiple dispersion regimes. Initial diffusion ($R^2 \propto t^1$) is followed by subdiffusion ($R^2 \propto t^{1/4}$), indicating eddy-limited motion. The population of the ensemble (number of feature pairs) is plotted on Y2.

selected for longevity above 50 ks or even (with somewhat wider standard error intervals) above 60 ks.

A natural explanation of the subdiffusive break is that the diffusive regime might occur within large, solar-originated eddies or stream boundaries that can entrain particles (Matthaeus & Goldstein 1986). The boundaries of such regions may form weak transport barriers for the solar wind plasma

fluid elements and thus inhibit the wide transport of test particles or cometary features.

The separation growth curve in Figure 4 rules out any regime of Batchelor diffusion or free streaming (in which $R^2 \propto t^2$) or of Richardson hyperdiffusion or unstable acceleration (in which $R^2 \propto t^3$) on timescales longer than the feature pickup time of 3–9 ks (Bourgoin et al. 2006).

The presence of the measured extended subdiffusive transport regime has important implications for interpretation of solar wind properties near Earth orbit. Using the fitted wind speed of 408 km s^{-1} , transit time from the Sun to 1 AU is 370 ks. Extrapolating the $t^{1/4}$ relationship out to 370 ks yields an estimated rms separation of 1 Gm in 2D or 700 Mm along the radial direction alone (assuming isotropy in the fluctuations). That separation corresponds to an rms crossing time of 1.7 ks for a fixed point near Earth.

Figure 5 shows evolution of the mean squared relative velocity $V^2 \equiv \langle \Delta v_x^2 + \Delta v_y^2 \rangle$ of the same feature pairs used for Figure 4. Because velocity measurements are noisier than direct displacement measurements, we have smoothed the V^2 data over a range of ± 3 samples (7 total) using a linear “tent” kernel; and the error bars remain relatively wider than for the corresponding displacement measurements. The image-plane rms speed of this pairwise relative motion begins at $120 \pm 10 \text{ km s}^{-1}$, corresponding to a pairwise speed of $150 \pm 12 \text{ km s}^{-1}$ in 3D and to $\sim 60 \text{ km s}^{-1}$ typical single particle speed in each coordinate direction.

The pickup interval of $6 \pm 3 \text{ ks}$ corresponds to a V^2 relaxation time (e -folding width) of $3 \pm 1.5 \text{ ks}$, so that by 9 ks V^2 is dominated by local variations in solar wind velocity rather than by the difference in release time between the features in

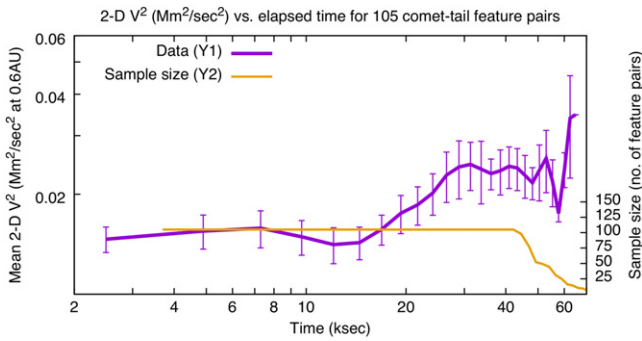


Figure 5. Evolution of the two-particle mean-squared relative speed function V^2 vs. elapsed time, for the comet-tail feature pairs in Figure 4, is consistent with velocity saturation after 30 ks, at a relative speed of $180 \pm 25 \text{ km s}^{-1}$. To reduce inherent noise in velocity measurement, the data are smoothed over a window of 10 ks.

each pair. After the pickup interval the pairwise relative speed gradually increases until 30 ks, saturating at $155 \pm 16 \text{ km s}^{-1}$ in the image plane ($190 \pm 20 \text{ km s}^{-1}$ in 3D). This “eddy speed” gives a typical turbulent energy per unit mass of $18 \pm 4 \text{ GJ kg}^{-1}$, or about 15%–25% of the kinetic energy associated with bulk motion of the solar wind at the location of the measurement. This value is in good agreement with observation and transport calculations for 1 AU, extrapolated inward to 0.4 AU (Padhye et al. 2001; Breech et al. 2008; Cranmer 2012).

Our inferred turbulent energy per unit mass is equivalent to a temperature of $\sim 2 \text{ MK}$ if fully randomized, $20\times$ larger than the $\sim 0.1 \text{ MK}$ temperature of the slow solar wind at 1 AU (Vasquez et al. 2007) and $7\times$ larger than the $\sim 0.3 \text{ MK}$ temperature of the fast wind (McComas et al. 2000). But the present observation does not cover the full range of scales: we are limited at large scales by the greatest rms separation observed, and at small scales by the inverse size of the (unresolved) features themselves. Similar limits apply in the temporal direction. We therefore speculate that the actual available kinetic energy at all fluctuation scales could be larger than what we measure, by a factor as high as 2. We conclude that the observed large scale fluctuating motion of the comet tail features reflects a sufficient reservoir of energy to heat the solar wind via dissipation, provided sufficiently strong cross-scale coupling to thermalize the energy.

Moreover, the high fluctuation speed implies that the inferred 700 Mm scale radial eddy structures at 1 AU should be very well mixed, with tens of eddy turnover times elapsed enroute between the Sun and Earth. We conclude that in-situ wind features up to a few times that size (with spacecraft crossing times of 1–2 hr) may be explained by turbulent mixing alone without regard for variability of the unknown solar wind source process. This high degree of mixing does not necessarily imply that the wind should be locally homogenized—only that rapid variations of wind parameters observed in situ largely reflect turbulent processing enroute, rather than indicating variability at the Sun.

3.3. Diffusion and Turbulent Energy

Using the R^2 data in Figure 4, we derived a one-dimensional diffusion coefficient $D_{xx} = (2.5 \pm 0.05) \text{ Mm}^2 \text{ s}^{-1}$ in the slow solar wind near 0.4 AU, in our observed diffusive regime of spatial scales up to $\sim 300 \text{ Mm}$. Here we derive the same value

independently from the evolution of V^2 and compare both values to prior measurements.

The comet tail features appear to follow a linear drag law, with a pickup time $\tau = 6 \pm 3 \text{ ks}$. This weak coupling acts as a linear low-pass filter on the solar wind variability: the tail features respond to the average motion of wind fluctuations on long timescales $t > \tau$, but the response is damped on timescales shorter than τ . An important consequence is that, during the pickup interval τ , each feature may sweep through several independent spatially local fluctuations in the solar wind, so that its deviation from the mean acceleration profile (and hence the shape of the overall two-particle V^2 function in the tail) depends on the statistics of these fluctuations.

The time for a correlated fluctuation in the solar wind to sweep past a fixed feature at the comet’s location may be estimated from the early V^2 variability and from our measured solar wind correlation length upper bound of 250 Mm. At a typical slow wind speed of 400 km s^{-1} , a correlation-length-sized feature sweeps past the feature in under 600 s, so that each comet tail feature experiences $\gtrsim 10$ independent fluctuation “hits” during the pickup process. Thus the Langevin statistical approach is applicable to the two-particle V^2 evolution during pickup: the V^2 evolution during this time can be considered as a form of Brownian motion superposed on the smooth acceleration of pickup.

In the Langevin regime, the one-dimensional diffusion coefficient D_{xx} approaches the value $\nu D_{xx} = \delta V_x^2 \tau$, where δV_x is the single particle, one-dimensional velocity dispersion (Chandrasekhar 1943). From Figure 5, the two-particle, two-dimensional V^2 is nearly constant before 15 ks, at $0.015 \pm 0.004 \text{ Mm}^2 \text{ s}^{-2}$. This corresponds to a δV_x of $61 \pm 8 \text{ km s}^{-1}$, and yields an independent, if crude, value $\nu D_{xx} = (22 \pm 18) \text{ Mm}^2 \text{ s}^{-1}$, inferred entirely from the statistics of V^2 . Given the simplicity of the model used (Van Kampen & Reinhardt 1983) and the wide confidence interval of the pickup time measurement, the order of magnitude agreement between D_{xx} and νD_{xx} may be considered as further supporting a general picture of scattering, pickup, transport, and spatial diffusion.

In diffusion theory the pickup time is identified with the Lagrangian correlation time of the random feature velocity field. Because we find no period of correlated motion in the features, this is an upper limit of the Lagrangian correlation time of the turbulence driving the fluctuations in feature motion. Multi-spacecraft observations from five spacecraft near 1 AU have yielded a solar wind frame estimate of the closely related Eulerian correlation time (Weygand et al. 2013). In the slow wind, Weygand et al. found $\tau_E \sim 13 \text{ ks}$ for slow wind. Assuming the timescale varies linearly with distance from the Sun, this corresponds to an estimated Lagrangian correlation time at 0.4 AU of 4 ks, which is consistent with our upper limit of $\tau = 6 \pm 3 \text{ ks}$.

4. DISCUSSION AND CONCLUSIONS

We have used visually identifiable features in the tail of a comet (Encke) as probes of the variable motion of the slow solar wind near 0.4 AU from the Sun. We accomplished this by analyzing the ensemble pairwise separation of ion tail features in the flow field of the solar wind. Because our measurement treats only a single interval in the solar wind, future similar analyses are required in different solar wind regimes to obtain a broader sample. An ideal measurement would include direct in-situ measurement of a comet tail for direct comparison of

spacecraft-frame data with the Lagrangian-frame analysis we demonstrated here. Nevertheless, direct Lagrangian analysis of wind flow by remote sensing is now possible with Encke and other comets (such as Pan-STARRS C/2011 L4) that present similar anomalous, compact ion tails.

Our measurements required exploiting cometary tail features as test particles in the solar wind. The Encke ion tail is slightly unusual among comets: while most cometary ion tails take on a “feathery” appearance as individual features spread along the local magnetic field, the individual features remain unusually compact for an ion tail. Similar compact tails have been observed on other comets, but are not the norm. For this reason, we carefully considered the hypothesis that they might be accelerated by radiation pressure, and ruled this out. Recent work by Raouafi et al. (2015) on Comet Pan-STARRS C/2011 L4 shows a train of similarly compact features, which they attribute to either dust or initially neutral Na, Li, K, or Ca atoms that could be picked up in a way similar to what we find for Encke.

Between radiation pressure, linear drag, or conventional (quadratic) hydrodynamic drag, the best-fit behavior is linear drag against the solar wind, with a best-fit pickup time of 6 ± 3 ks, comfortably shorter than the interval before our observed crossover from random walk diffusion to eddy driven subdiffusion. During the pickup interval, the random walk we observe is in part due to spatial variation in flow as the particles cross through different uncorrelated streams, as well as to local temporal variation in flow from turbulence (which continues after pickup). The inferred diffusion coefficient is the same in both regimes and is consistent with turbulent speeds and correlation times from spacecraft frame measurements at 1 AU.

There is also reasonable consistency between the velocity and displacement data, and the expected theoretical relationship between the velocity diffusion and spatial transport (Chandrasekhar 1943). This lends support to the use of comet tail features as solar wind tracers.

We found that there is no visible free-streaming or unstable hyperdiffusive behavior in the solar wind, in our observable separation intervals >200 Mm. We did find strong evidence of uncorrelated random-walk behavior between nearby test particles at scales up to 400 Mm, with semiconfined (eddy) motion at larger scales up to our observation’s limit of 65 ks from cometary release.

We infer that the semiconfined ($R^2 \propto t^{1/4}$) motion is caused by eddies or similar structures in the wind, and that the slow solar wind undergoes large-scale turbulent processing and mixing enroute to Earth.

We conclude that on timescales up to about 2 hr (6 ks), variability in the “quiet” slow solar wind near Earth is primarily due to mixing within the inferred subdiffusive eddies as the wind propagates from Sun to Earth. On these short to moderate timescales, features identified in the wind likely reflect turbulent fluctuations, rather than remnants of variability in the source process at the Sun.

The kinetic energy of fluctuations associated with this turbulence is approximately 20% of the kinetic energy of the bulk solar wind flow, in agreement with prior estimates from in-situ fixed-frame point measurements, and may be as much as a factor of two higher still. This is more than $10\times$ the energy reservoir required to heat the solar wind to observed temperatures at 1AU.

Dissipation of turbulent energy has been measured in-situ at small scales with many experiments including the *Cluster*

mission (e.g., Leamon et al. 1998; Vasquez et al. 2007; Sahraoui et al. 2009). Our direct measurement of the large-scale end of the turbulent cascade complements that work by demonstrating that there is sufficient available energy to drive the observed small-scale dissipation and maintain the hot solar wind to 1 AU and beyond, while still maintaining a turbulent flow field.

We note that, because the comet tail remnants are quite dense compared to the solar wind, they may affect the local solar wind turbulence by adding sufficient ponderous mass to damp short timescale turbulent motions in the wind that entrains them. We do not quantify this effect directly, but note that (A) it applies preferentially to small scale eddy motions rather than the large scale motions we have characterized in this work; (B) the direction of the effect is toward underestimation of turbulent fluctuation amplitudes; and (C) the observed bulk speed of the tail after pickup is quite close to both accepted and our fitted values of the solar wind speed, indicating that the tail is in fact being picked up by the bulk flow of the wind on the timescales we measured. We conclude that our primary results are robust: large-scale turbulence mixes the solar wind on crossing timescales up to 1–2 hr; and the turbulence entrains sufficient kinetic energy to heat the solar wind, if the cross-scale coupling is strong enough to dissipate the energy.

The authors gratefully acknowledge support from NASA grants NNX12AM99G and NNX14AI63G, and NSF grants AGS1063439 and AGS1156094, and also from the NSF-supported REU program administered by the University of Colorado. They also thank D. J. McComas for valuable discussions as the work developed. Further, the work was significantly improved by suggestions made by the anonymous referee, and we are grateful for the input. Thanks also to the *STEREO* mission team for making their data widely available in many places including <http://stereo-ssc.nascom.nasa.gov>. The analysis made extensive use of the freeware Perl Data Language (PDL), available at <http://pdl.perl.org>.

REFERENCES

- Alfvén, H. 1957, *Tellus*, **9**, 92
- Bourgoin, M., Ouellette, N. T., Xu, H., Berg, J., & Bodenschatz, E. 2006, *Sci*, **311**, 835
- Breech, B., Matthaeus, W. H., Minnie, J., et al. 2008, *JGRA*, **113**, 8105
- Buffington, A., Bisi, M. M., Clover, J. M., et al. 2008, *ApJ*, **677**, 798
- Chae, J., Schühle, U., & Lemaire, P. 1998, *ApJ*, **505**, 957
- Chandrasekhar, S. 1943, *RvMP*, **15**, 1
- Clover, J. M., Jackson, B. V., Buffington, A., Hick, P. P., & Bisi, M. M. 2010, *ApJ*, **713**, 394
- Cranmer, S. R. 2012, *SSRv*, **172**, 145
- Cranmer, S. R., Field, G. B., & Kohl, J. L. 1999, *ApJ*, **518**, 937
- DeForest, C. E., Howard, T. A., & Tappin, S. J. 2011, *ApJ*, **738**, 103
- Elliott, H. A., Henney, C. J., McComas, D. J., Smith, C. W., & Vasquez, B. J. 2012, *JGRA*, **117**, 9102
- Eyles, C. J., Harrison, R. A., Davis, C. J., et al. 2009, *SoPh*, **254**, 387
- Fisk, L. A., Schwadron, N. A., & Zurbuchen, T. H. 1999, *JGR*, **104**, 19765
- Gombosi, T. I., Powell, K. G., & de Zeeuw, D. L. 1994, *JGR*, **99**, 21525
- Howard, R. A., Moses, J. D., Vourlidis, A., et al. 2008, *SSRv*, **136**, 67
- Jackson, B. V., Buffington, A., Clover, J. M., et al. 2013, in AIP Conf. Ser. 1539, SOLAR WIND 13: Proc. of the Thirteenth International Solar Conf., ed. G. P. Zank et al. (Melville, NY: AIP), 364
- Jokipii, J. R. 1966, *ApJ*, **146**, 480
- Kolmogorov, A. N. 1941, *DoSSR*, **32**, 16
- Kuchar, T. A., Buffington, A., Arge, C. N., et al. 2008, *JGRA*, **113**, 4101
- Kuchar, T. A., Mizuno, D., Arge, C. N., et al. 2004, AGU Fall Meeting Abstracts, abstract SH21A-0396
- Leamon, R. J., Smith, C. W., Ness, N. F., Matthaeus, W. H., & Wong, H. K. 1998, *JGR*, **103**, 4775

- Mäkinen, J. T. T., Silén, J., Schmidt, W., et al. 2001, *Icar*, **152**, 268
- Matthaeus, W. H., & Goldstein, M. L. 1986, *PhRvL*, **57**, 495
- Matthaeus, W. H., & Velli, M. 2011, *SSRv*, **160**, 145
- McComas, D. J., Barraclough, B. L., Funsten, H. O., et al. 2000, *JGR*, **105**, 10419
- Mullan, D. J. 1991, *A&A*, **248**, 256
- Neugebauer, M., & Snyder, C. W. 1966, *JGR*, **71**, 469
- Padhye, N. S., Smith, C. W., & Matthaeus, W. H. 2001, *JGR*, **106**, 18635
- Parker, E. N. 1958, *ApJ*, **128**, 664
- Pope, S. B. 2000, *Turbulent Flows* (London: Cambridge Univ. Press)
- Raouafi, N.-E., Lisse, C. M., Stenborg, G., Jones, G. H., & Schmidt, C. A. 2015, arXiv:1507.02579
- Raymond, J. C., Kohl, J. L., Noci, G., et al. 1997, *SoPh*, **175**, 645
- Ruiz, M. E., Dasso, S., Matthaeus, W. H., & Weygand, J. M. 2014, *SoPh*, **289**, 3917
- Sahraoui, F., Goldstein, M. L., Robert, P., & Khotyaintsev, Y. V. 2009, *PhRvL*, **102**, 231102
- Shalchi, A. (ed.) 2009, *Nonlinear Cosmic Ray Diffusion Theories* (Vol. 362; Berlin: Springer)
- Suess, S. T., Poletto, G., Wang, A.-H., Wu, S. T., & Cuseri, I. 1998, *SoPh*, **180**, 231
- Tu, C.-Y., & Marsch, E. 1995, *SSRv*, **73**, 1
- Van Kampen, N. G., & Reinhardt, W. P. 1983, *PhT*, **36**, 78
- Vasquez, B. J., Smith, C. W., Hamilton, K., MacBride, B. T., & Leamon, R. J. 2007, *JGRA*, **112**, 7101
- Vourlidas, A., Davis, C. J., Eyles, C. J., et al. 2007, *ApJL*, **668**, L79
- Wang, Y.-M., Bierstecker, J. B., Sheeley, N. R., Jr., et al. 2007, *ApJ*, **660**, 882
- Wang, Y.-M., Sheeley, N. R., Jr., Walters, J. H., et al. 1998, *ApJL*, **498**, L165
- Weygand, J. M., Matthaeus, W. H., Kivelson, M. G., & Dasso, S. 2013, *JGRA*, **118**, 3995
- Whipple, F. L. 1972, in *Proc. of the Twenty-First Symp., From Planet to Planet*, ed. A. Elvius (New York: Wiley), 211
- Woo, R., & Martin, J. M. 1997, *GeoRL*, **24**, 2535
- Zirker, J. B. 1977, *RvGSP*, **15**, 257